

Opportunistic Localization of Underwater Robots using Drifters and Boats

Filippo Arrichiello, Hordur K. Heidarsson, Gaurav S. Sukhatme

Abstract—The paper characterizes the performance of Autonomous Underwater Vehicle (AUV) localization when the AUV moves in environments where floating drifters or surface vessels are present and can be used for relative localization. In particular, we study how localization performance is affected by parameters e.g. surface object density, their visibility range and their motion. We present a discrete-time nonlinear model for an AUV equipped with onboard sensors and relative positioning information from surface objects (e.g., ranging and bearing) and derive the associated relative Posterior Cramér-Rao Lower Bound. We introduce a probabilistic motion model for the AUV, based on a random direction mobility model, to analyze the expected performance of the localization algorithm in terms of hitting time between the AUV and the surface objects. Finally, an extensive simulation analysis is performed using a discrete time Extended Kalman Filter with Maximum-Likelihood Data Association. As a proof of concept, an AUV equipped with an upward looking sonar is shown to detect a surface vessel and improve its localization estimate.

I. INTRODUCTION

Autonomous Underwater Vehicles (AUVs) are increasingly used for both scientific purposes and commercial applications due to their ability to navigate in environments hostile to humans, or to perform relatively long term missions (e.g., of the order of weeks for underwater gliders). Despite their appealing features, the navigation problem has been not completely solved due to several technological and theoretical constraints. Indeed, while diving, AUVs can neither rely on GPS signals nor on exteroceptive sensors such as cameras, due to scarce visibility range and/or reduced number of reference features. Thus, AUV navigation is performed relying on dead-reckoning techniques that estimate the position using on-board sensors (compass, Inertial Measurement Unit (IMU), Doppler Velocity Log (DVL)). However, since dead-reckoning techniques suffer numerical drift due to uncertainties and integration of noisy sensor information, they are useful for relatively short paths. After a certain amount of time, the AUV is usually required to surface to get an absolute position fix via GPS before starting a new dive.

Acoustic localization systems are becoming prominent due to the possibility they offer for absolute localization of AUVs while diving. Different commercial solutions are Long, Short, and Ultra-Short Baseline (LBL, SBL, USBL). In LBL, the AUV makes use of range measurements from fixed nodes in known positions, gained via the time of flight of acoustic messages, and applies trilateration algorithms to

estimate its position. In SBL, three or more transducers are mounted on a surface vessel, and a trilateration algorithm is used to estimate AUV position. SBL requires less infrastructure (compared to LBL) but the operational area is reduced and the localization accuracy may be lower. In USBL, a set of transducers is assembled in a single device usually installed on board a support ship, and the AUV position is estimated measuring the relative phases between the signals arriving at the transducers. This solution is compact and does not require further infrastructure, however, the positioning accuracy and robustness can be less than for the previous methods. Moreover, SBL and USBL need to transmit the estimated position back to the AUV.

In this paper we consider the case of **opportunistic localization**, that is the case where ad-hoc localization solutions are lacking but the AUV moves in an environment where drifting buoys and surface vessels are present and can be used for relative localization. The aim of the paper is to characterize the localization of the AUV with respect to few key parameters: the number of drifters or vessels in a certain area, their visibility range and some sensor and process parameters. In particular, two scenarios for the relative localization are studied. In the first, the AUV uses acoustic communication for both range measurement and information exchange with the drifters/vessels (giving rise to a range-only localization problem); in the second scenario, the AUV is able to recognize surface objects using an upward looking sonar (a range-bearing localization problem). In the second scenario we assume that the absolute position of the drifters/vessels is received via acoustic communication or, for the drifter case, estimated using current models e.g., ROMS (Regional Ocean Model System) or Great Lakes Operational Forecast System (GLOFS).

With this idea in mind, we introduce a discrete-time nonlinear model for the system (that includes both range-only and range-bearing localization). Since we do not want to focus our study on a specific localization filter, we make use of an iterative formulation of the Posterior Cramér-Rao Lower Bound (PCRL) to evaluate the theoretical performance of an unbiased localization filter. We consider a random direction mobility model for the AUV, and characterize the localization algorithms based on the expected hitting time (that is the expected time the AUV navigates without seeing any reference feature). We discuss the data association problem for the range-bearing case and develop an Extended Kalman Filter with Maximum Likelihood Data Association (EKF-MLDA). An extensive numerical analysis is performed to study the behavior of the system in different scenarios. Finally, as a proof of concept, we present preliminary experimental results

F. Arrichiello is with the Department DAEIMI of the University of Cassino, via G. Di Biasio 43, 03043 Cassino (FR), Italy f.arrichiello@unicas.it

H.K. Heidarsson and G.S. Sukhatme are with the Robotic Embedded Systems Laboratory, University of Southern California, Los Angeles, CA 90089, USA [{heidarss,gaurav}@usc.edu">f.heidarss,gaurav}@usc.edu](mailto)

obtained with an AUV (the EcoMapper) localizing itself using an upward looking sonar to utilize relative range and bearing to an autonomous surface vessel equipped with GPS.

II. RELATED WORK

A wide overview on AUV modeling, navigation and control can be found in e.g. [1], while interesting state of the art navigation technologies for AUVs can be found in [16]. The recent paper [8] reports the state of the art of model-aided inertial navigation system for underwater vehicles, while [10] describes a six degree of freedom AUV navigation approach with IMU, LBL, DVL. The paper [5] presents an approach, alternative to standard LBL triangulation techniques, for AUV localization within a field of surface floating buoys; the approach is based on a set-membership technique and considers unknown but bounded measurement errors.

There are many research efforts on single-beacon AUV localization, i.e., localization using one single transponder/transducer couple for range measurement, integrating information coming from on board sensors (depth measurement, inertial velocity or acceleration measurement from DVL or IMU). Among the different approaches, a solution to the single-beacon localization problem in the presence of unknown currents is presented in [7], while different filtering approaches, together with experimental tests with an autonomous surface vessel and an underwater vehicle, are presented in [6]. Field experiments in deep water using an EKF for the single beacon localization are presented in [19].

In this paper we use the recursive formulation of Posterior Cramér-Rao Lower Bound (PCRLB) for discrete time nonlinear filtering presented in [18]. Recent papers on this subject deal with recursive formulation to estimate on-line the PCRLB. For example, in [9] an online approximate estimation of the PCRLB for discrete time nonlinear filtering, using the mean and covariance of the estimated online state instead of the true state, is presented. A different approximate recursive formula to calculate conditional PCRLB for nonlinear/non-Gaussian Bayesian estimation is presented in [20]. Considering the specific subject of our paper, the inspiring work [4] presents a study, based on CRLB, on AUV positioning uncertainty prediction using LBL and DVL.

Random mobility models have been used in different robotic applications, e.g., achieving connectivity of mobile robot networks through coalescence [12], [13] or searching for a target that intermittently emits signals [14]. An overview on random mobility models as random waypoint, random walk, non-uniform spatial distribution and random direction can be found in the survey [2]. Properties of the random direction model can be found in [11], while [15] presents an analytical derivation of hitting time, meeting time and contact time for random direction.

III. MODELING

Let $\Sigma_I : \{O - X_I, Y_I, Z_I\}$ be a inertial, Earth-fixed, reference frame defined according to the North East Down (NED) convention. By the assumption that the AUV directly measures its depth and it has auto-stabilized roll, we neglect

the vertical component and model the AUV with an under-actuated 2D discrete time kinematic non linear model, whose state vector is given by:

$$\mathbf{x}_k = [x_{k-1} \ y_{k-1} \ \theta_{k-1} \ x_k \ y_k \ \theta_k]^T \in \mathbb{R}^6 \quad (1)$$

where x_i , y_i , and θ_i are respectively the cartesian coordinates in the inertial reference frame and the yaw at the i^{th} instant (see fig. 1), and with the state equation:

$$\mathbf{x}_{k+1} = \mathbf{A}\mathbf{x}_k + \mathbf{B}(\mathbf{x}_k)\mathbf{u}_k + \mathbf{F}(\mathbf{x}_k)\mathbf{w}_k \quad (2)$$

$$\text{where } \mathbf{A} = \begin{bmatrix} \mathcal{O}_{3 \times 3} & \mathcal{I}_{3 \times 3} \\ \mathcal{O}_{3 \times 3} & \mathcal{I}_{3 \times 3} \end{bmatrix}; \mathbf{B}(\mathbf{x}_k) = \begin{bmatrix} \mathcal{O}_{3 \times 2} & 0 \\ dT \cos(\theta_k) & 0 \\ dT \sin(\theta_k) & 0 \\ 0 & dT \end{bmatrix};$$

\mathbf{u} is the input vector $\mathbf{u} = [v_k \ \omega_k]^T \in \mathbb{R}^2$ with v and ω noting the linear velocity in the surge direction and the

yaw rate, respectively; $\mathbf{F}(\mathbf{x}_k) = \begin{bmatrix} \mathcal{O}_{3 \times 2} \\ \cos(\theta_k) & 0 \\ \sin(\theta_k) & 0 \\ 0 & 1 \end{bmatrix}$; \mathbf{w}_k is the process noise assumed to be zero-mean Gaussian

$\mathbf{w}_k \sim \mathcal{N}(0, \mathbf{R}_w)$ with covariance $\mathbf{R}_w = \begin{bmatrix} \sigma_{w,v}^2 & 0 \\ 0 & \sigma_{w,\omega}^2 \end{bmatrix}$. We also assume that the system has a constant sample time dT .

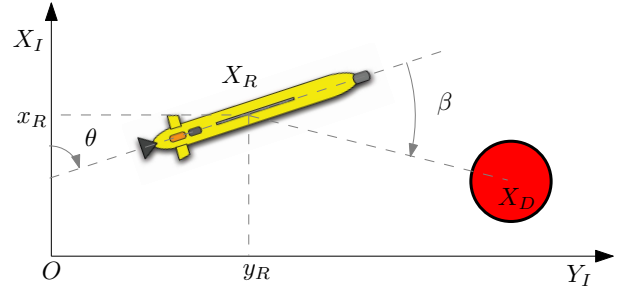


Fig. 1. Reference system and notation.

We assume that the AUV is equipped with proprioceptive sensors and relative localization sensors that can be employed depending on the specific operational mode. We define a sensor model and linearization for each of them. These will be used for computing the PCRLB and the implementation of the EKF-MLDA. We assume the noise to be unbiased for both process and sensor models.

A. Compass

The compass gives information about the actual yaw of the AUV, thus

$$y_{Comp} = \theta_k + v_{Comp} \quad (3)$$

where the noise is supposed zero-mean Gaussian, i.e., $v_{Comp} \sim \mathcal{N}(0, \sigma_{Comp}^2)$. The output linearization matrix is obtained deriving the output function w.r.t. the state components, thus it yields:

$$\mathbf{C}_{Comp} = [0 \ 0 \ 0 \ 0 \ 0 \ 1]. \quad (4)$$

B. Doppler Velocity Log/Inertial Measurement Unit

The AUV is assumed to be equipped with a DVL/IMU to measure linear and angular velocity. In a discrete time formulation, its output, including the effect of the sample time dT , is given by:

$$\mathbf{y}_{DVL} = [x_k - x_{k-1} \quad y_k - y_{k-1} \quad \theta_k - \theta_{k-1}]^T + \mathbf{v}_{DVL} \quad (5)$$

where the noise is $\mathbf{v}_{DVL} \sim \mathcal{N}(0, \mathbf{R}_{v,DVL})$. To consider the common behavior of the DVL of having different covariance in the surge, sway and yaw direction, the covariance matrix is assumed to be:

$$\mathbf{R}_{v,DVL} = \begin{bmatrix} \mathcal{R}(\theta) \begin{bmatrix} \sigma_{DVL,x}^2 & 0 \\ 0 & \sigma_{DVL,y}^2 \end{bmatrix} \mathcal{R}^T(\theta) & 0 \\ 0 & \sigma_{DVL,\theta}^2 \end{bmatrix}, \quad (6)$$

where $\mathcal{R}(\theta)$ is a proper 2D rotation matrix. The output linearization matrix assumes the form:

$$\mathbf{C}_{DVL} = [-\mathcal{I}_{3 \times 3} \quad \mathcal{I}_{3 \times 3}] \quad (7)$$

C. Range from Drifter

With a mild abuse of terminology, in the following we use the term drifter for a generic feature on the surface (thus, both a drifter and a boat). Assuming that the AUV can measure its range from a drifter in position $\mathbf{X}_D = [x_D, y_D]^T$ and defining the AUV position as $\mathbf{X}_R = [x_k, y_k]^T$, then the output equation is

$$y_{Range} = \|\mathbf{X}_D - \mathbf{X}_R\| + \mathbf{v}_{Range} \quad (8)$$

where $\mathbf{v}_{Range} \sim \mathcal{N}(0, \sigma_{Range}^2)$ is the zero-mean Gaussian error. The output linearization matrix assume the form:

$$\mathbf{C}_{Range} = \begin{bmatrix} 0 & 0 & 0 & \frac{x_k - x_D}{\|\mathbf{X}_D - \mathbf{X}_R\|} & \frac{y_k - y_D}{\|\mathbf{X}_D - \mathbf{X}_R\|} & 0 \end{bmatrix} \quad (9)$$

D. Bearing of the Drifter

The bearing measurement β_k represents the direction of the relative position vector $\mathbf{X}_D - \mathbf{X}_R$ in the AUV body fixed reference frame. Thus, it yields

$$y_{Bear} = \beta_k + \mathbf{v}_{Bear} = \text{atan2}(y_D - y_k, x_D - x_k) - \theta_k + \mathbf{v}_{Bear} \quad (10)$$

with $\mathbf{v}_{Bear} \sim \mathcal{N}(0, \sigma_{Bear}^2)$ and output linearization matrix:

$$\mathbf{C}_{Bear} = \begin{bmatrix} 0 & 0 & 0 & -\frac{y_D - y_k}{\|\mathbf{X}_D - \mathbf{X}_R\|^2} & \frac{x_D - x_k}{\|\mathbf{X}_D - \mathbf{X}_R\|^2} & -1 \end{bmatrix} \quad (11)$$

IV. RANGE-BEARING AND RANGE-ONLY LOCALIZATION

With a proper selection of the available outputs we can use the previous models for both range-bearing and range-only localization (in this paper we do not consider bearing-only localization). We assume that compass and DVL/IMU are activated in both the cases. For range-bearing localization, we assume two measurements $[y_{Range}, y_{Bear}]_j$ are available

for each of the m drifters in the AUV visibility range. Thus,

$$\mathbf{y} = \begin{bmatrix} \mathbf{y}_{DVL} \\ y_{Comp} \\ y_{Range} \\ y_{Bear} \end{bmatrix}_1 + \mathbf{v} = \begin{bmatrix} x_k - x_{k-1} \\ y_k - y_{k-1} \\ \theta_k - \theta_{k-1} \\ \theta_k \\ \|\mathbf{X}_D - \mathbf{X}_R\| \\ \beta_k \\ \vdots \\ \|\mathbf{X}_D - \mathbf{X}_R\| \\ \beta_k \end{bmatrix}_1 + \mathbf{v} \quad (12)$$

where $\mathbf{v} \sim \mathcal{N}(0, \mathbf{R}_v)$ and where

$$\mathbf{R}_v = \text{diag}(\mathbf{R}_{v,DVL}, \sigma_{Comp,\theta}^2, \text{diag}(\sigma_{Range}^2, \sigma_{Bear}^2)_{1 \dots m})$$

$$\mathbf{C} = \begin{bmatrix} -1 & 0 & 0 & 1 & 0 & 0 \\ 0 & -1 & 0 & 0 & 1 & 0 \\ 0 & 0 & -1 & 0 & 0 & 1 \\ 0 & 0 & 0 & 0 & 0 & 1 \\ 0 & 0 & 0 & -\frac{x_k - x_D}{\|\mathbf{X}_D - \mathbf{X}_R\|} & \frac{y_k - y_D}{\|\mathbf{X}_D - \mathbf{X}_R\|} & 0 \\ 0 & 0 & 0 & -\frac{y_D - y_k}{\|\mathbf{X}_D - \mathbf{X}_R\|^2} & \frac{x_D - x_k}{\|\mathbf{X}_D - \mathbf{X}_R\|^2} & -1 \end{bmatrix}_1 \quad (13)$$

In the case of range-only localization with a single drifter in the visibility range, the output is simply $\mathbf{y} = [y_{DVL} \quad y_{Comp} \quad y_{Range}]^T + \mathbf{v}$.

V. LOCALIZATION ALGORITHM POSTERIOR CRAMÉR-RAO LOWER BOUND

To evaluate the theoretical performance of a localization algorithm we derive the Posterior Cramér-Rao Lower Bound for our system that gives the performance limits for any unbiased estimator. In particular, for a discrete time non-linear system

$$\mathbf{x}_{k+1} = \mathbf{f}_k(\mathbf{x}_k, \mathbf{u}_k, \mathbf{w}_k); \quad \mathbf{w}_j \sim \mathcal{N}(0, \mathbf{R}_w) \quad (14)$$

$$\mathbf{y}_k = \mathbf{h}_t(\mathbf{x}_k, \mathbf{v}_k); \quad \mathbf{v}_k \sim \mathcal{N}(0, \mathbf{R}_v) \quad (15)$$

it is well known that, given a set of n measurements $\mathbf{Y}_n = (\mathbf{y}_0, \dots, \mathbf{y}_n)$, the sequence of states $\mathbf{X}_k = (\mathbf{x}_0, \dots, \mathbf{x}_k)$ and their estimates $\hat{\mathbf{X}}_k = (\hat{\mathbf{x}}_0, \dots, \hat{\mathbf{x}}_k)$, the covariance of any estimator cannot go below a bound

$$E[(\mathbf{X}_k - \hat{\mathbf{X}}_k)(\mathbf{X}_k - \hat{\mathbf{X}}_k)^T] \geq \mathbf{J}^{-1}(\mathbf{X}_k) \quad (16)$$

where $\mathbf{J}(\mathbf{X}_k)$ is the Fisher Information Matrix

$$\mathbf{J}(\mathbf{X}_k) = E \left(\frac{-\partial^2}{\partial \mathbf{X}_k \partial \mathbf{X}_k} \log p(\mathbf{X}_k, \mathbf{Y}_k) \right). \quad (17)$$

However, in the filtering context we are generally interested in the right lower block \mathbf{J}_k of $\mathbf{J}(\mathbf{X}_k)$, that gives information of the estimate of \mathbf{x}_k , which is given by

$$\mathbf{J}_k \triangleq (\mathcal{C}_k - \mathcal{B}_k^T \mathcal{A}_k^{-1} \mathcal{B}_k) \quad (18)$$

where

$$\mathcal{A}_k = -E \left[\frac{\partial^2}{\partial \mathbf{X}_{k-1} \partial \mathbf{X}_{k-1}} \log p(\mathbf{X}_k, \mathbf{Y}_k) \right] \quad (19)$$

$$\mathcal{B}_k = -E \left[\frac{\partial^2}{\partial \mathbf{X}_{k-1} \partial \mathbf{x}_k} \log p(\mathbf{X}_k, \mathbf{Y}_k) \right] \quad (20)$$

$$\mathcal{C}_k = -E \left[\frac{\partial^2}{\partial \mathbf{x}_k \partial \mathbf{x}_k} \log p(\mathbf{X}_k, \mathbf{Y}_k) \right] \quad (21)$$

Tichavsky et al. [18] give an elegant recursive formulation to obtain J_k :

$$\mathbf{J}_{k+1} = \mathcal{D}_k^{22} - \mathcal{D}_k^{21} (\mathbf{J}_k + \mathcal{D}_k^{11})^{-1} \mathcal{D}_k^{12} \quad (22)$$

where

$$\mathcal{D}_k^{11} = -E \left[\frac{\partial^2}{\partial \mathbf{x}_k^2} \log p(\mathbf{x}_{k+1} | \mathbf{x}_k) \right] \quad (23)$$

$$\mathcal{D}_k^{12} = (\mathcal{D}_k^{21})^T = -E \left[\frac{\partial^2}{\partial \mathbf{x}_k \partial \mathbf{x}_{k+1}} \log p(\mathbf{x}_{k+1} | \mathbf{x}_k) \right] \quad (24)$$

$$\begin{aligned} \mathcal{D}_k^{22} = & -E \left[\frac{\partial^2}{\partial \mathbf{x}_{k+1}^2} \log p(\mathbf{x}_{k+1} | \mathbf{x}_k) \right] + \\ & + E \left[\frac{\partial^2}{\partial \mathbf{x}_{k+1}^2} \log p(\mathbf{y}_{k+1} | \mathbf{x}_{k+1}) \right]. \end{aligned} \quad (25)$$

If the noise of the system is additive and Gaussian, this yield:

$$\mathcal{D}_k^{11} = E \left[\mathcal{A}_k^T \mathbf{R}_{k,w}^{-1} \mathcal{A}_k \right] \quad (26)$$

$$\mathcal{D}_k^{12} = (\mathcal{D}_k^{21})^T = -E \left[\mathcal{A}_k^T \right] \mathbf{R}_{k,w}^{-1} \quad (27)$$

$$\mathcal{D}_k^{22} = \mathbf{R}_{k,w}^{-1} + E \left[\mathcal{C}_{k+1}^T \mathbf{R}_{v,k+1}^{-1} \mathcal{C}_{k+1} \right] \quad (28)$$

where $\mathcal{A}_k = \frac{\partial \mathbf{f}_k}{\partial \mathbf{x}}(\mathbf{x}_k, \mathbf{u}_k)$, $\mathcal{C}_{k+1} = \frac{\partial \mathbf{h}_{k+1}}{\partial \mathbf{x}}(\mathbf{x}_{k+1})$. Thus, eq. (22) becomes:

$$\begin{aligned} \mathbf{J}_{k+1} = & \mathbf{R}_{k,w}^{-1} + E \left[\mathcal{C}_{k+1}^T \mathbf{R}_{v,k+1}^{-1} \mathcal{C}_{k+1} \right] - \mathbf{R}_{k,w}^{-1} E \left[\mathcal{A}_k \right] * \\ & * \left(\mathbf{J}_k + E \left[\mathcal{A}_k^T \mathbf{R}_{k,w}^{-1} \mathcal{A}_k \right] \right)^{-1} E \left[\mathcal{A}_k^T \right] \mathbf{R}_{k,w}^{-1} \end{aligned} \quad (29)$$

Assuming that the system in eq. (2) has additive process noise, we can rewrite it as

$$\mathbf{x}_{k+1} = \mathbf{A} \mathbf{x}_k + \mathbf{B}(\mathbf{x}_k) \mathbf{u}_k + \mathbf{w}_v \quad (30)$$

where $\mathbf{w}_k \sim \mathcal{N}(0, R_w)$ with

$\mathbf{R}_w = \text{diag}([\sigma_{v,x,k-1}^2, \sigma_{v,y,k-1}^2, \sigma_{v,\theta,k-1}^2, \sigma_{v,x,k}^2, \sigma_{v,y,k}^2, \sigma_{v,\theta,k}^2])$. Thus, it yields

$$\begin{aligned} \mathcal{A}_k = & \mathbf{A} + \frac{\partial \mathbf{B}_k \mathbf{u}_k}{\partial \mathbf{x}}(\mathbf{x}_k, \mathbf{u}_k) = \\ = & \begin{bmatrix} 0 & 0 & 0 & 1 & 0 & 0 \\ 0 & 0 & 0 & 0 & 1 & 0 \\ 0 & 0 & 0 & 0 & 0 & 1 \\ 0 & 0 & 0 & 1 & 0 & -v_k dt \sin(\theta_k) \\ 0 & 0 & 0 & 0 & 1 & v_k dt \cos(\theta_k) \\ 0 & 0 & 0 & 0 & 0 & 1 \end{bmatrix} \end{aligned} \quad (31)$$

$$\mathcal{C}_k = \mathbf{C}_k \quad (32)$$

To report the output in an additive noise formulation we apply a change of coordinate to the DVL output so that, for

the range-bearing case, we get:

$$\mathbf{y} = \begin{bmatrix} (x_k - x_{k-1}) \cos(\theta_k) + (y_k - y_{k-1}) \sin(\theta_k) \\ -(x_k - x_{k-1}) \sin(\theta_k) + (y_k - y_{k-1}) \cos(\theta_k) \\ \theta_k - \theta_{k-1} \\ \theta_k \\ \|\mathbf{X}_D - \mathbf{X}_R\| \\ \beta_k \end{bmatrix} + \mathbf{v} \quad (33)$$

and $\mathbf{v} \sim \mathcal{N}(0, R_v)$, with

$\mathbf{R}_v = \text{diag}([\sigma_{DVL,x}^2, \sigma_{DVL,y}^2, \sigma_{DVL,\theta}^2, \sigma_{Comp}^2, \sigma_{Range}^2, \sigma_{Bear}^2])$.

In the following numerical simulations we will refer to eq. (29) together with eq. (31-32) with \mathcal{C}_k calculated w.r.t eq. (33). It is worth noting that, since some terms of eq. (29) are functions of the expected values, we can not use a closed form formulation and we have to resort to, e.g., Monte Carlo numerical simulations to derive the filter performance.

VI. MOBILITY MODEL

As evident from eq. (29), the performance of the system is affected by the available onboard sensors and their covariances, the number of drifters in the visibility range of the AUV, their displacement, and the kind of available relative localization measurements (range-only or range-bearing). When no drifters are in its visibility range, the AUV relies solely on dead-reckoning (using DVL/IMU and compass), and, as well known, the covariance of the position estimation increases with a rate depending on sensor covariance and process noise; instead, the estimation covariance quickly decreases as soon as a drifter is detected. In this section we characterize the frequency with which the AUV 'sees' (i.e. either obtains a range-bearing pair to the drifter or the range to the drifter) a drifter depending on some key parameters.

We study the problem in the simplified case of a random mobility model for the AUV and extract the expected values of the variables of interest. In particular, we assign an epoch-based random direction model to the AUV, that is, during each epoch, the robot moves in a fixed direction at a constant velocity; at the beginning of each epoch, the motion direction θ_d as well as the epoch duration T and the velocity ν are randomly chosen according to a distribution (specified below). We define L as the length of the path covered during an epoch. At the end of each epoch, the AUV may eventually remain still for a time T_{stop} (e.g., to achieve a sampling operation in a given location). Moreover, the AUV is assumed to be constrained to move inside an assigned area of dimension Ar where there are n_{dr} drifters with maximum visibility range K . When the AUV reaches the boundaries of the area, it is reflected back by specularly changing its motion direction.

We assume that the random motion parameters of each epoch are chosen as follows:

- θ_d is chosen uniformly random in $[0, 2\pi]$
- the speed ν is randomly chosen from $[\nu_{min}, \nu_{max}]$ with average values $\bar{\nu}$
- the epoch length L is chosen as a random variable with expected value $\bar{L} = O(\sqrt{Ar})$

- the epoch duration T is chosen from an exponential distribution with average L/ν ; the expected epoch duration is denoted as $\bar{T} = E[L/\nu]$
- after T time units the AUV pauses for a random amount of time chosen between $[0, T_{max}]$, with average T_{stop}

Assigning such parameters, we can extract the expected hitting time, meeting time or contact duration. The hitting time gives an information about the mean time the robot moves without seeing any drifters (in a scenario with stationary drifters e.g., moored buoys). The expected meeting time, conversely, is the time the robot navigates without seeing any drifters when the drifters themselves are moving with a similar random direction motion with a mean velocity $\bar{\nu}_D$. The contact time is the time the robot remains in the visibility range of the drifters. The expected values of these parameters can be calculated following the treatment in [15]; here we report the main formulas for hitting and meeting times:

- **Expected hitting time**

$$ET = \left(\frac{Ar}{2K\bar{L}n_{dr}} \right) \left(\frac{\bar{L}}{\bar{\nu}} + \bar{T}_{stop} \right) \quad (34)$$

- **Expected meeting time**

$$EM = \frac{ET}{p_m\hat{\nu} + 2(1 - p_m)}, \quad (35)$$

where $\hat{\nu}$ is the normalized relative speed, and $p_m = \bar{T}/(\bar{T} + \bar{T}_{stop})$ is the probability that the robot is moving. Given the drifter mean velocity $\bar{\nu}_D$ and given $k = \bar{\nu}_D/\bar{\nu}$, then $\hat{\nu} = \frac{\bar{\nu}}{2\pi} \int_0^{2\pi} \sqrt{1 + k^2 - 2k \cos(\theta)} d\theta$.

VII. EXTENDED KALMAN FILTER WITH MAXIMUM LIKELIHOOD DATA ASSOCIATION

Beyond the theoretical performance of the PCRLB, we want to test the localization performance with a common filtering technique; thus, we developed a discrete time Extended Kalman Filter with Maximum Likelihood Data Association (EKF-MLDA). Indeed, when multiple drifters are simultaneously in the AUV's visibility range, data association problems could arise, that is, due to estimation uncertainties, the AUV is not able to properly associate the relative measurements to the corresponding drifters. The data association problem could arise for the range-bearing localization when the AUV, equipped with the upward looking sonar and having a prediction of drifter positions (e.g., estimated via an ocean model or received directly from the drifters via acoustic communication), has to correlate uncertain data from sonar with the uncertain map of drifter positions. In range-only localization, we neglect the data association problem since we assume that the range measurement is obtained directly using the acoustic communication; in this case it is reasonable assuming that the acoustic communication allows exchanging messages with both GPS position and the drifters' ID. In the latter case we use a classical discrete time EKF.

The data association problem has been widely studied in the literature, e.g. see [3], and in this paper we refer to a solution inherited from [17]. In particular, the EKF-MLDA

has been implemented using the following equations:

- 1) **Time update of state and estimation error covariance:**

$$\hat{\mathbf{x}}_{k+1}^- = \mathbf{A}\hat{\mathbf{x}}_k^+ + \mathbf{B}(\hat{\mathbf{x}}_k^+) \bar{\mathbf{u}} \quad (36)$$

$$\mathbf{P}_{k+1}^- = \mathbf{A}\mathbf{P}_k^+ \mathbf{A}^T + \mathbf{F}(\hat{\mathbf{x}}_k^+) \mathbf{R}_w \mathbf{F}(\hat{\mathbf{x}}_k^+)^T \quad (37)$$

- 2) **Measurement updates of state and estimation error covariance with MLDA:**

Supposing the AUV has N_D drifters in its visibility range, then, the EKF measurement vector is:

$$\mathbf{y}_i = [\mathbf{y}_{DVL}^T \quad \mathbf{y}_{Comp}^T \quad \mathbf{y}_{D,1}^T \quad \dots \quad \mathbf{y}_{D,N_D}^T] \quad (38)$$

where $\mathbf{y}_{D,i} = [y_{Range,i} \quad y_{Bear,i}]^T$ is the range-bearing measurement of each seen drifter. We define the vector

$$\hat{\mathbf{y}}_{D,j} = \begin{bmatrix} y_{Range}(\mathbf{X}_{D,j}, \hat{\mathbf{x}}_{k+1}^-) \\ y_{Bear}(\mathbf{X}_{D,j}, \hat{\mathbf{x}}_{k+1}^-) \end{bmatrix} \quad (39)$$

and the matrix

$$\hat{\mathbf{C}}_{D,j} = \begin{bmatrix} \mathbf{C}_{Range}(\mathbf{X}_{D,j}, \hat{\mathbf{x}}_{k+1}^-) \\ \mathbf{C}_{Bear}(\mathbf{X}_{D,j}, \hat{\mathbf{x}}_{k+1}^-) \end{bmatrix} \quad (40)$$

as the estimated measurements and output linearization matrix obtained by using the drifter position $\mathbf{X}_{D,j}$ and the AUV position estimate $\hat{\mathbf{x}}_{k+1}^-$. We solve the data association problem, coupling the i^{th} -drifter \mathbf{X}_{D,i_M} to the i^{th} -measurement, based on their maximum likelihood; thus, we use the following pseudo-code

for $j = 1 \rightarrow N_D$ **do**

$$\mathbf{S}_j = \hat{\mathbf{C}}_{D,j} \mathbf{P}_{k+1}^- \hat{\mathbf{C}}_{D,j}^T + \mathbf{R}_v$$

end for

$$i_M = \underset{j}{\operatorname{argmax}} \frac{1}{|2\pi\mathbf{S}_j|} e^{\{-\frac{1}{2}(\mathbf{y}_{D,i} - \hat{\mathbf{y}}_{D,j})^T [\mathbf{S}_j]^{-1} (\mathbf{y}_{D,i} - \hat{\mathbf{y}}_{D,j})\}}$$

then we build the matrix

$$\bar{\mathbf{C}} = [\mathbf{C}_{DVL}^T \quad \mathbf{C}_{Comp}^T \quad \hat{\mathbf{C}}_{D,1,M}^T \quad \dots \quad \hat{\mathbf{C}}_{D,N_D,M}^T]^T \quad (41)$$

Once the data association is done, the remaining EKF equations are as follows:

$$\mathbf{K}_{k+1} = \mathbf{P}_{k+1}^- \bar{\mathbf{C}}^T [\bar{\mathbf{C}} \mathbf{P}_{k+1}^- \bar{\mathbf{C}}^T + \mathbf{R}_v]^{-1} \quad (42)$$

$$\tilde{\mathbf{y}}_{k+1} = \mathbf{y}_k - \mathbf{h}(\mathbf{x}_{k+1}^-, \mathbf{X}_{D,1,M}, \dots, \mathbf{X}_{D,N_D,M}) \quad (43)$$

$$\hat{\mathbf{x}}_{k+1}^+ = \hat{\mathbf{x}}_{k+1}^- + \mathbf{K}_{k+1} \tilde{\mathbf{y}}_{k+1} \quad (44)$$

$$\mathbf{P}_{k+1}^+ = (\mathbf{I} - \mathbf{K}_{k+1} \bar{\mathbf{C}}(\mathbf{x}_{k+1}^-)) \mathbf{P}_{k+1}^- \quad (45)$$

VIII. SIMULATION STUDY

In this section we present the results of a simulation analysis of range-only and range-bearing localization algorithms with the set of parameters chosen as in Table I.

In order to show the main behaviors of PCRLB and of the EKF for the two different localization problems, we start by running two simulations where the AUV, initialized in position $[0 \quad 0]$ m, moves along a straight path of 500 m in presence of a single drifter in position $[250 \quad 80]$ m and with visibility range equal to 100 m. Figure 2 shows the path of the AUV and the covariance ellipsoid obtained considering the x_k, y_k components from the \mathbf{J}_k^{-1} matrix. It is worth noticing that, as soon the AUV enters the visibility range

TABLE I
SIMULATIONS PARAMETERS

$\sigma_{v,x,k} = \sigma_{v,y,k} = 1$	$\sigma_{v,\theta,k-1} = .05$
$\sigma_{v,x,k-1} = \sigma_{v,y,k-1} = .005$	$\sigma_{v,\theta,k-1} = .0005$
$\sigma_{DVL,x} = \sigma_{DVL,y} = 5$	$\sigma_{DVL,\theta} = (4/180 * \pi)$
$\sigma_{Comp} = (2/180 * \pi)$	$\sigma_{Range} = 1$
$\sigma_{Bear} = .01$	$dT = 5$
$L = 1000$	$\bar{v} = 1m/s$
$J_1 = (P)^{-1} = .2 * I_6$	$T_{stop} = 0$

of the drifter, the covariance ellipsoid quickly reduces its component only along the drifter radial direction. Figure 3 shows the estimation error of the EKF, the distance between the AUV and the drifter, and the eigenvalues of the 3x3 lower right submatrix of J_k^{-1} .

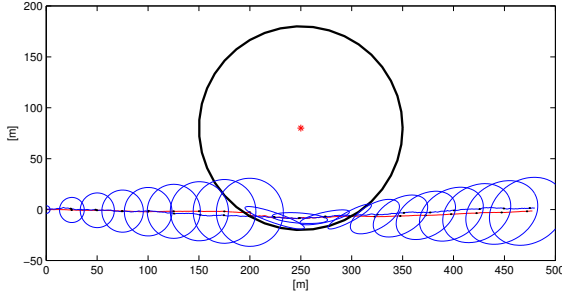


Fig. 2. Range-only localization: path and covariance ellipsoid of a AUV navigating in presence of a single drifter.

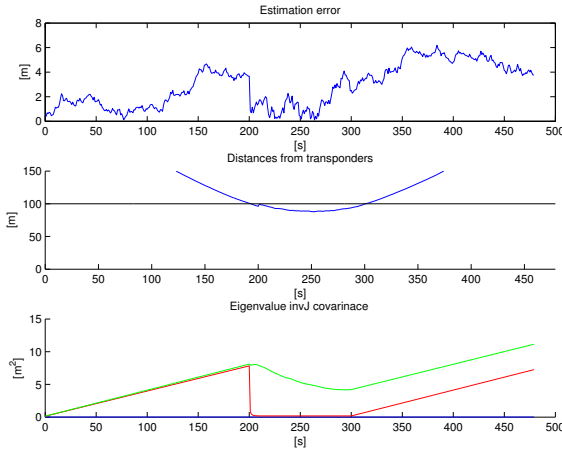


Fig. 3. Range-only localization: a) EKF estimation error b) distance from the drifter c) eigenvalues of the 3x3 lower right submatrix of J_k^{-1} .

Figures 4 and 5 show analogous results for the range-bearing case. Notice that, in this case, both the eigenvalues of the covariance matrix given by the x_k, y_k components from the J_k^{-1} decrease simultaneously as soon as the drifter information are available.

A. Varying Drifter Density

As an illustrative example, we show the results of two simulations at low/high drifter density. Figure 6 shows the path of a range-bearing localization simulation where the AUV navigated in a bounded area of $3 \times 3 \text{ km}^2$ in presence of 5 drifters with visibility range $K = 500 \text{ m}$. The figure shows the AUV path, the estimated path and the drifters visibility area. Figure 7 shows the measured hitting times,

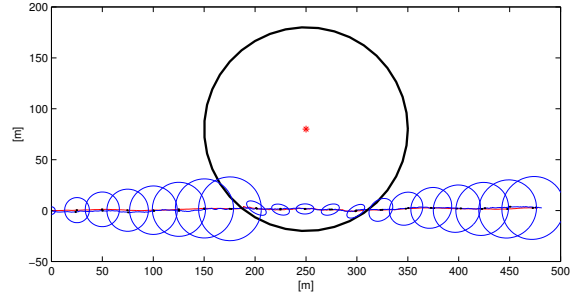


Fig. 4. Range-bearing localization: path and covariance ellipsoid of a AUV navigating in presence of a single drifter.

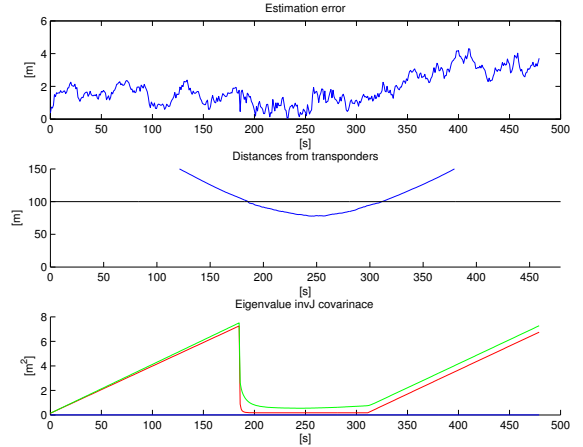


Fig. 5. Range-bearing localization: a) EKF estimation error b) distance from the drifter c) eigenvalues of the 3x3 lower right submatrix of J_k^{-1} .

their mean value and the expected value calculated via eq. (34). Equivalent results for a scenario with higher drifter

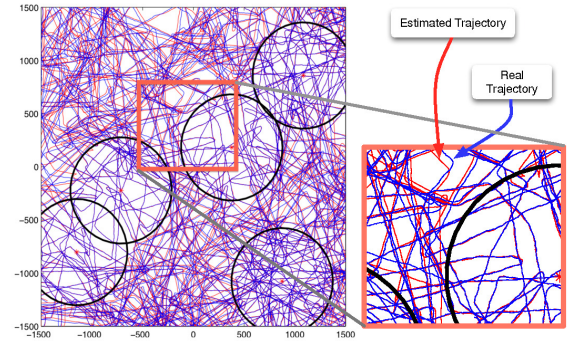


Fig. 6. Range-bearing localization: navigation in presence of 5 randomly placed drifters. Real and estimated AUV trajectories; drifters visibility areas. density (20 drifters) are shown in figures 8 and 9.

B. Statistical Analysis

With the same environment as the previous simulations, we present the results of extensive simulations with different numbers of stationary/moving drifters. Figures 10 and 11 show the mean hitting time and the mean covariance eigenvalues (of both EKF and PCLRB) with an increasing number of drifters; the mean values are obtained by performing each simulation 20 times with a fixed number of drifters but each time placing them randomly according to a uniform distribution (each simulation lasted 3000s). The left plots

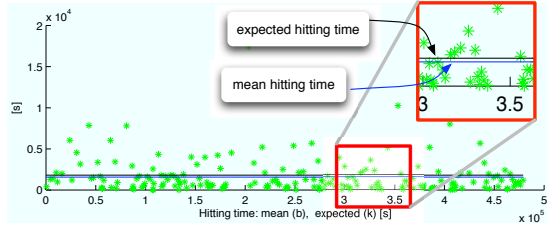


Fig. 7. Range-bearing localization: measured, mean and expected hitting times in presence of 5 randomly placed drifters.

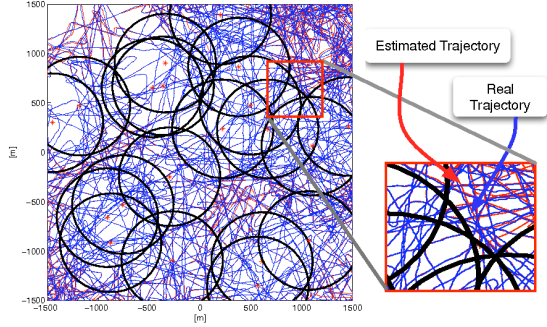


Fig. 8. Range-bearing localization: navigation in presence of 20 randomly placed drifters. Real and estimated AUV trajectories; drifters visibility areas.

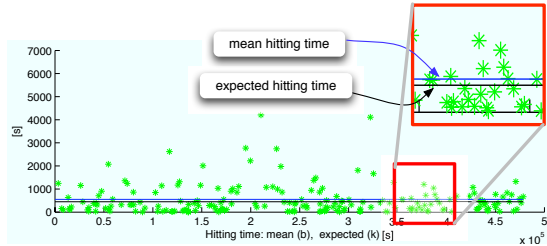


Fig. 9. Range-bearing localization: measured, mean and expected hitting times in presence of 20 randomly placed drifters.

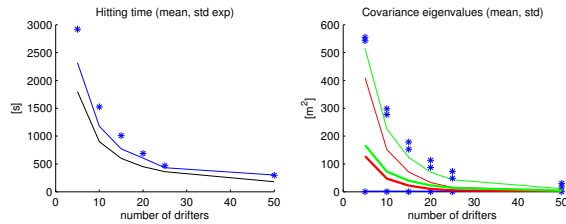


Fig. 10. Range-only localization with different numbers of stationary drifters. a) mean (blue) and expected (black) hitting times b) mean eigenvalues of the covariance matrix for EKF (thin line) and PCLB (thick line).

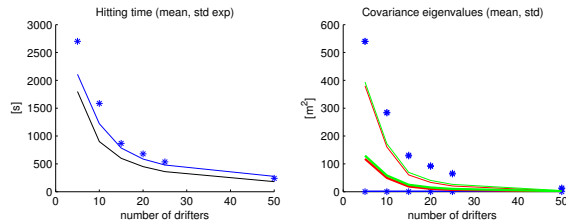


Fig. 11. Range-bearing localization with different numbers of stationary drifters: a) mean (blue) and expected (black) hitting times b) mean eigenvalues of the covariance matrix for EKF (thin line) and PCLB (thick line).

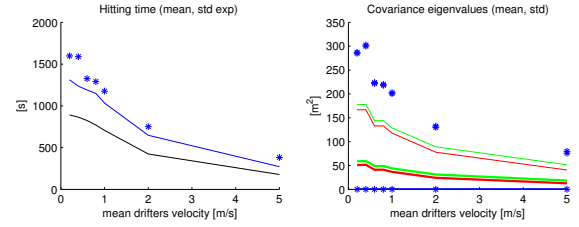


Fig. 12. Range-bearing localization in presence of 10 drifters moving with different mean velocities: a) mean (blue) and expected (black) hitting time b) mean eigenvalues of the covariance matrix for EKF (thin line) and PCLB (thick line).

show the mean and the expected hitting time, while the right plots show the mean eigenvalues of the covariance matrix of both EKF and PCRLB for both range-only and range-bearing localization. Figure 12 shows the analogous values with drifters moving with increasing velocity.

IX. PRELIMINARY FIELD EXPERIMENTS

In this section we present preliminary experiments with an AUV and an Autonomous Surface Vessel (see Figure 13).

The AUV, namely the EcoMapper, is a torpedo style vehicle designed and manufactured by YSI Inc. The vehicle has a three blade propeller and four independent control planes and it is capable of speeds ranging from 0.5 - 2 m/s, with an endurance of around 8 hours. It is equipped with GPS, compass, pressure sensor and a DVL for navigation, as well as with a side-scan sonar (that, for the specific experiment, was mounted in an upward looking configuration) and a suite of water quality sensors. Communication with the vehicle is limited to WiFi when on the surface.

The Autonomous Surface Vessel is an OceanScience QBoat-I hull, with a length of 2.1 m and a width of 0.7 m at the widest section, equipped with an onboard computer. The vehicle was equipped with a uBlox EKF-5H GPS that provides global position updates at 2 Hz, and a Microstrain 3D-M IMU with integrated compass sampled at 50 Hz.

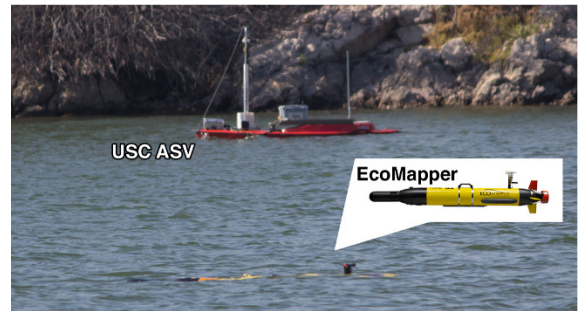


Fig. 13. Experimental testbed composed of an ASV and an AUV with upward looking sonar.

The AUV was commanded to perform different dives at a constant depth of 3 m in a bounded area where the ASV was present. The experiments were designed to study the capability of the AUV to estimate the position of the ASV using the upward looking sonar. Trials were performed with different sonar frequency configurations, 330 kHz and 800 kHz, with the ASV moving and stationary. Figure 15 shows the path obtained postprocessing the data from AUV and

ASV during one of the runs. The AUV performed two dives of about 100m recording sonar images. The figure shows both the paths estimated with dead-reckoning (DVL, compass) and with the EKF using range and bearing to the ASV obtained using the sonar images and the AUV depth; the initial estimation error is assumed null in both the case. To appreciate the performance of the EKF, the figure shows, as a ground truth, the path obtained fusing GPS (available when the AUV is on the surface), DVL, and compass information. The EKF gives an estimate much closer to the real AUV path than the dead-reckoning. Figure 15 shows a snapshot of the runs, in the instant the AUV was able to detect the ASV. The attached video shows a 3D reconstruction from the experimental data of the paths followed by the AUV and the ASV, the side scan sonar images acquired during the same dives, and the estimated paths. Future experiments will focus on the testing AUV localization in presence of multiple ASVs and drifters.

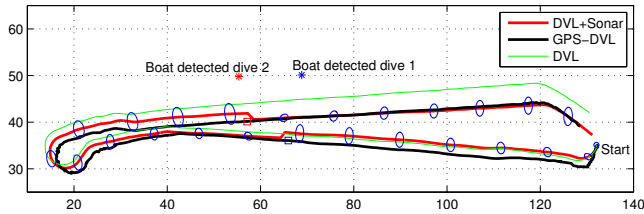


Fig. 14. Path reconstructions from experimental data: dead-reckoning (green), dead-reckoning + sonar measurement (red), GPS + DVL (black).

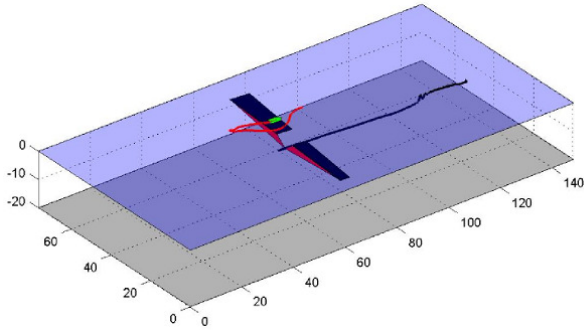


Fig. 15. Experimental data reconstruction when the AUV detects the ASV.

X. CONCLUSION

In this paper we address an opportunistic localization problem for underwater robots in presence of drifters and surface vessels. The idea is to allow the AUV to take advantage of relative measurements of range (or range and bearing) to drifters or surface vessels present in the area. The surface vehicles' positions are assumed to be accurately known (GPS) allowing the AUV to improve its self-localization estimate each time it 'sees' a surface vessel or a drifter. We study how localization performance is affected by parameters such as drifter density, drifter visibility range and drifter motion. We present a discrete-time nonlinear model for an AUV localizing itself using onboard sensors and relative positioning information from surface objects (e.g., ranging and bearing) and derive the associated relative

Posterior Cramér-Rao Lower Bound. Based on a random walk motion model, we analyze the expected performance of the localization algorithm in terms of hitting time between the AUV and the surface objects. An extensive simulation analysis is performed using a discrete time Extended Kalman Filter with Maximum-Likelihood Data Association. A preliminary implementation in which an AUV equipped with an upward looking sonar detects a surface vessel and improves its localization estimate is presented.

REFERENCES

- [1] G. Antonelli, T. Fossen, and D. Yoerger. *Springer Handbook of Robotics*, chapter Underwater Robotics, pages 987–1008. B. Siciliano, O. Khatib, (Eds.), Springer-Verlag, Heidelberg, D, 2008.
- [2] F. Bai and A. Helmy. A survey of mobility models. *Wireless Adhoc Networks*. University of Southern California, USA, 2004.
- [3] Y. Bar-Shalom and E. Tse. Tracking in a cluttered environment with probabilistic data association. *Automatica*, 11(5):451–460, 1975.
- [4] B. Bingham. Predicting the navigation performance of underwater vehicles. In *2009 IEEE/RSJ Int. Conf. on Intelligent Robots and Systems*, pages 261–266, 2009.
- [5] A. Caiti, A. Garulli, F. Livide, and D. Prattichizzo. Localization of autonomous underwater vehicles by floating acoustic buoys: a set-membership approach. *IEEE Jour. of Oceanic Engineering*, 30(1):140–152, 2005.
- [6] M.F. Fallon, G. Papadopoulos, J.J. Leonard, and N.M. Patrikalakis. Cooperative AUV navigation using a single maneuvering surface craft. *The Int. Jour. of Robotics Research*, 29(12):1461–1474, 2010.
- [7] A.S. Gadre and D.J. Stilwell. A complete solution to underwater navigation in the presence of unknown currents based on range measurements from a single location. In *2005 IEEE/RSJ Int. Conf. on Intelligent Robots and Systems*, pages 1420–1425, 2005.
- [8] O. Hegrenæs and O. Hallingstad. Model-aided ins with sea current estimation for robust underwater navigation. *IEEE Jour. of Oceanic Engineering*, 36(2):316–337, 2011.
- [9] M. Lei, B.J. van Wyk, and Y. Qi. Online estimation of the approximate posterior cramer-rao lower bound for discrete-time nonlinear filtering. *IEEE Tran. on Aerospace and Electronic Systems*, 47(1):37–57, 2011.
- [10] P.A. Miller, J.A. Farrell, Y. Zhao, and V. Djapic. Autonomous underwater vehicle navigation. *IEEE Jour. of Oceanic Engineering*, 35(3):663–678, 2010.
- [11] P. Nain, D. Towsley, B. Liu, and Z. Liu. Properties of random direction models. In *IEEE INFOCOM 2005*, volume 3, pages 1897–1907, 2005.
- [12] S. Poduri and G.S. Sukhatme. Achieving connectivity through coalescence in mobile robot networks. In *1st Int. Conf. on Robot communication and coordination*, pages 1–6, 2007.
- [13] S. Poduri and G.S. Sukhatme. Latency analysis of coalescence for robot groups. In *IEEE Int. Conf. on Robotics and Automation*, pages 3295–3300, 2007.
- [14] D. Song, C.-Y. Kim, and J. Yi. On the time to search for an intermittent signal source under a limited sensing range. *IEEE Tran. on Robotics*, 27(2):313–323, April 2011.
- [15] T. Spyropoulos, A. Jindal, and K. Psounis. An analytical study of fundamental mobility properties for encounter-based protocols. *Int. Jour. of Autonomous and Adaptive Communications Systems*, 1(1):4–40, 2008.
- [16] L. Stutters, H. Liu, C. Tiltman, and D.J. Brown. Navigation technologies for autonomous underwater vehicles. *IEEE Tran. on Systems, Man, and Cybernetics, Part C: Applications and Reviews*, 38(4):581–589, 2008.
- [17] S. Thrun, W. Burgard, and D. Fox. *Probabilistic robotics*. MIT Press, 2001.
- [18] P. Tichavsky, C.H. Muravchik, and A. Nehorai. Posterior cramer-rao bounds for discrete-time nonlinear filtering. *IEEE Tran. on Signal Processing*, 46(5):1386–1396, 1998.
- [19] S.E. Webster, R.M. Eustice, H. Singh, and L.L. Whitcomb. Preliminary deep water results in single-beacon one-way-travel-time acoustic navigation for underwater vehicles. In *2009 IEEE/RSJ Int. Conf. on Intelligent Robots and Systems*, pages 2053–2060, 2009.
- [20] L. Zuo, R. Niu, and P.K. Varshney. Conditional posterior cramer-rao lower bounds for nonlinear sequential bayesian estimation. *IEEE Tran. on Signal Processing*, 59(1):1–14, 2011.